PFC/JA-88-48

CYLINDRICAL BRILLOUIN FLOW IN RELATIVISTIC SMOOTH-BORE MAGNETRONS

Ronald C. Davidson
George L. Johnston
Kang T. Tsang*
Adam T. Drobot*

December, 1988

Plasma Fusion Center
Massachusetts Institute of Technology
Cambridge, MA 02139

*Science Applications International Corp.
8200 Greensborough Drive, McLean, VA 22102

CYLINDRICAL BRILLOUIN FLOW IN RELATIVISTIC SMOOTH-BORE MAGNETRONS

Ronald C. Davidson and George L. Johnston
Plasma Fusion Center, Massachusetts Institute of Technology
167 Albany Street, Cambridge, Massachusetts 02139

Kang T. Tsang and Adam T. Drobot
Science Applications International Corporation
8200 Greensborough Drive, McLean, Virginia 22102

ABSTRACT

A macroscopic cold-fluid model is used to determine the influence of cylindrical effects on the operating range and properties of the electron flow in relativistic smooth-bore magnetrons. Assuming operation at Brillouin flow, it is found that cylindrical effects (such as the centrifugal force on an electron fluid element) can significantly modify several features of the equilibrium flow and diode operating range relative to the case of planar flow.

1. INTRODUCTION

In relativistic magnetrons,[1-6] pulsed, high-voltage diodes (operating in the MV range, say) are used to generate microwaves at gigawatt power levels. While magnetically insulated electron flow[7,8] and related features of the magnetron instability[9-13] have been extensively analyzed in planar geometry, there are relatively few theoretical treatments that attempt to retain the full influence of self-field and cylindrical effects (centrifugal force effects, finite diode aspect ratio, etc.) on the diode operating range and equilibrium profiles[14] as well as stability behavior.[15,16] In this paper, a macroscopic cold-fluid model is used to determine the detailed influence of cylindrical effects on the operating range and properties of the equilibrium electron flow in relativistic smooth-bore magnetrons. Assuming operation at Brillouin flow, the normalized layer thickness and Hull cut-off voltage are calculated over a wide range of diode aspect ratio $a/(b - a)$, and normalized fill field $eB_f(b - a)/mc^2$.

2. THEORETICAL MODEL

In the present analysis, we make use of a macroscopic cold-fluid model[14] to investigate equilibrium properties of relativistic, non-

neutral electron flow in the cylindrical smooth-bore magnetron configuration illustrated in Fig. 1. All equilibrium properties are assumed to be azimuthally symmetric ($\partial/\partial\theta = 0$) and independent of axial coordinate ($\partial/\partial z = 0$). The cathode is located at $r = a$, the anode is located at $r = b$, and space-charge-limited flow is assumed with

$$\phi_0(r = a) = 0 \text{ and } \phi_0(r = b) = V, \qquad E_r(r = a) = 0 \ . \tag{1}$$

Here, V is the applied voltage, $\phi_0(r)$ is the electrostatic potential, and $E_r(r) = -\partial\phi_0/\partial r$ is the radial electric field. The combined radial electric field $E_r(r)\hat{\underset{\sim}{e}}_r$ and axial magnetic field $B_z(r)\hat{\underset{\sim}{e}}_z$ produce an equilibrium rotation of the nonneutral electron fluid with normalized azimuthal flow velocity

$$\beta_b(r) = V_{\theta b}(r)/c = \omega_b(r)r/c \ , \tag{2}$$

where c is the speed of light <u>in vacuo</u>. It is assumed that the equilibrium density profile $n_b(r)$ extends from the cathode at $r = a$ to radius $r = r_b$ (the outer edge of the electron layer), and that the region $r_b < r \leq b$ corresponds to a vacuum region. The electric and magnetic fields are determined self-consistently from

$$\frac{1}{r}\frac{\partial}{\partial r} rE_r(r) = -4\pi e n_b(r) \ , \tag{3}$$

$$\frac{\partial}{\partial r} B_z(r) = 4\pi e n_b(r)\beta_b(r) \ , \tag{4}$$

where $-e$ is the electron charge. In the subsequent analysis, the applied magnetic field in the vacuum region is denoted by

$$B_z(r) = B_0 = \text{const.}, \quad r_b < r \leq b \ . \tag{5}$$

To complete the macroscopic cold-fluid equilibrium description, Eqs.(3) and (4) are supplemented by the radial force balance equation

$$-\gamma_b(r)\beta_b^2(r) = -\frac{e}{mc^2}\left[rE_r(r) + \beta_b(r)rB_z(r)\right] \ , \tag{6}$$

where m is the electron rest mass, and

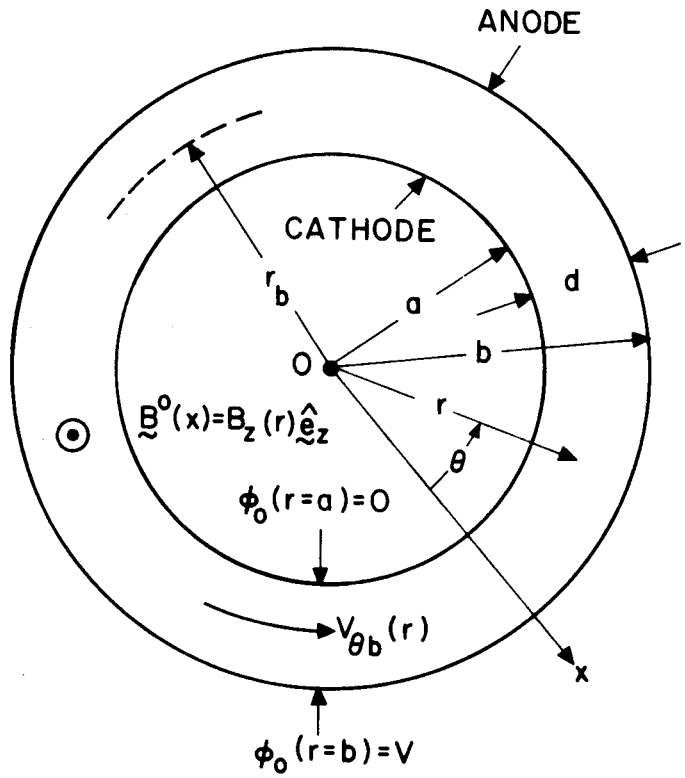

Fig. 1. Cylindrical smooth-bore magnetron.

$$\gamma_b(r) = [1 - \beta_b^2(r)]^{-1/2} \tag{7}$$

is the relativistic mass factor. Consistent with $E_r(r = a) = 0$ in Eq.(1), we consider the class of solutions to Eq.(6) in which there is zero flow velocity at the cathode, i.e.,

$$\beta_b(r = a) = 0 \ . \tag{8}$$

Equations (3), (4) and (6), supplemented by the boundary conditions in Eqs.(1), (5) and (8), can be used to calculate the equilibrium profiles $E_r(r)$, $B_z(r)$, $n_b(r)$ and $\beta_b(r)$. Generally speaking, there is considerable latitude in the choice of equilibrium profiles in a macroscopic cold-fluid model.[14] For example, the radial dependence of any one of the profiles $E_r(r)$, $B_z(r)$, $n_b(r)$ and $\beta_b(r)$ can be prescribed arbitrarily, and the three remaining profiles calculated self-consistently from Eqs.(3), (4) and (6).

3. CYLINDRICAL BRILLOUIN FLOW EQUILIBRIUM

In the present analysis, we assume that the total electron energy is equal to zero across the layer profile, i.e.,

$$[\gamma_b(r) - 1]mc^2 - e\phi_0(r) = 0 \ , \tag{9}$$

which corresponds to Brillouin flow. Taking the derivative of Eq.(9) with respect to r gives

$$\frac{e}{mc^2} E_r(r) = -\frac{\partial}{\partial r}\gamma_b = -\gamma_b^3\beta_b \frac{\partial}{\partial r}\beta_b \ , \tag{10}$$

where use has been made of Eq.(7). Combining Eqs. (3), (4), (6), (9) and (10), we obtain the closed equation

$$\frac{\beta_b}{r}\frac{\partial}{\partial r}\left(r\frac{\partial\gamma_b}{\partial r}\right) = \frac{\partial}{\partial r}\left[\frac{\gamma_b\beta_b^2 + r\partial\gamma_b/\partial r}{r\beta_b}\right] , \tag{11}$$

where $\gamma_b = (1 - \beta_b^2)^{-1/2}$. The second-order differential equation (11) is to be solved for $\beta_b(r)$ over the radial extent of the electron layer ($a \leq r < r_b$). Because $\beta_b(r = a) = 0$ and $\gamma_b(r = a) = 1$, we find from Eqs.(10) and (11) that

$$\left[\frac{\partial\beta_b}{\partial r}\right]^2_{r=a} = \frac{4\pi n_b(r = a)e^2}{mc^2} \equiv \frac{\omega_{pb}^2(a)}{c^2} \ . \tag{12}$$

Similarly, it can be shown that

$$\omega_{pb}^2(a) = \frac{e^2B_z^2(r = a)}{m^2c^2} \equiv \omega_c^2(a) \ , \tag{13}$$

which corresponds to the familiar Brillouin-flow condition at the cathode.

It is convenient to express Eq.(11) in an alternate form by introducing the flow parameter $\chi_b(r)$ defined by

$$\beta_b(r) = \tanh\chi_b(r) \ . \tag{14}$$

Making use of Eq.(14) and $\gamma_b(r) = (1 - \beta_b^2)^{-1/2} = \cosh\chi_b(r)$, we find that Eq.(11) can be expressed in the equivalent form

$$\frac{1}{r}\frac{\partial}{\partial r}\left(r\frac{\partial \chi_b}{\partial r}\right) = \frac{\sinh\chi_b\cosh\chi_b}{r^2} . \tag{15}$$

Consistent with Eq.(12) and $\beta_b(r = a) = 0$, Eq.(15) is to be solved subject to the boundary conditions

$$\chi_b(r = a) = 0 ,$$

$$\left[\frac{\partial \chi_b}{\partial r}\right]^2_{r=a} = \frac{\omega_{pb}^2(a)}{c^2} \equiv \kappa^2 . \tag{16}$$

Integrating Eq.(15) with respect to r, we obtain

$$\left(r\frac{\partial \chi_b}{\partial r}\right)^2 = \kappa^2 a^2 + \sinh^2\chi_b , \tag{17}$$

where the boundary conditions in Eq.(16) have been enforced.

Equation (17) is the final equation describing equilibrium Brillouin flow in cylindrical diode geometry. In this regard, Eq.(17) is applicable within the electron layer ($a \leq r < r_b$) and must be solved subject to the boundary condition $\chi_b(r = a) = 0$, which corresponds to $\beta_b(r = a) = 0$. Numerical solutions to Eq.(17) are presented in Fig. 2, where $\chi_b(r)$ is plotted versus $\kappa(r - a)$ for several choices of the dimensionless parameter κa. As a general remark, for large aspect ratio and a thin layer satisfying

$$\begin{aligned} \kappa^2 a^2 &\gg \sinh^2\chi_b , \\ (r_b - a)^2 &\ll a^2 , \end{aligned} \tag{18}$$

it is readily shown that the solution to Eq.(17) reduces to the familiar planar result[11]

$$\chi_b(r) = \kappa(r - a) , \tag{19}$$

which corresponds to normalized flow velocity $\beta_b(r) = \tanh[\kappa(r - a)]$ within the electron layer ($a \leq r < r_b$). When Eq.(18) is not satisfied, it is clear from Fig. 2 that the cylindrical effects in Eq.(17) can significantly modify the solution for $\chi_b(r)$ relative to the planar result in Eq.(19).

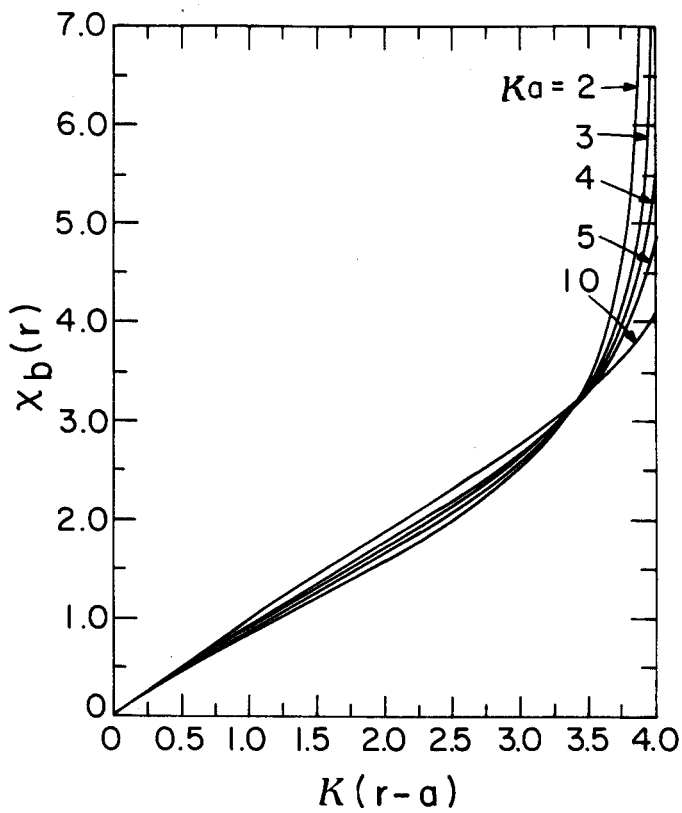

Fig. 2. Plots of χ_b versus $\kappa(r - a)$ obtained from Eq.(17) for several values of κa.

4. VOLTAGE AND FILL-FIELD CONDITIONS

The equilibrium electric and magnetic field profiles, $E_r(r)$ and $B_z(r)$, are readily expressed in terms of $\chi_b(r)$ by making use of Eqs.(3) and (4). Without presenting algebraic details, we integrate Poisson's equation (3) from $r = a$ to $r = b$ and enforce $\phi_0(r = b) = V$, where V is the applied voltage at the anode. This gives

$$\frac{eV}{mc^2} = [\cosh\chi_b - 1]_{r=r_b} + \left[r\sinh\chi_b \frac{\partial\chi_b}{\partial r}\right]_{r=r_b} \ln\left(\frac{b}{r_b}\right), \qquad (20)$$

which relates $\chi_b(r = r_b)$ and $[\partial\chi_b/\partial r]_{r=r_b}$ at the surface of the electron layer to the normalized voltage eV/mc^2. Furthermore, we make use of magnetic flux conservation, $2\pi\int_a^b dr r B_z$ = const., to relate the initial fill field B_f (assumed to be uniform prior to formation of the electron layer) to the magnetic field depression after the

layer is formed. Making use of $eB_z/mc^2 = r^{-1}(\partial/\partial r)(r\sinh\chi_b)$ within the electron layer ($a \leq r < r_b$), we obtain

$$\frac{eB_f(b-a)}{mc^2} = \frac{(b^2+r_b^2)}{r_b(b+a)}\,[\sinh\chi_b]_{r=r_b} + \frac{(b^2-r_b^2)}{r_b(b+a)}\left[r\cosh\chi_b\,\frac{\partial\chi_b}{\partial r}\right]_{r=r_b} . \tag{21}$$

Equations (20) and (21) relate eV/mc^2 and $eB_f(b-a)/mc^2$ to r_b, $\chi_b(r=r_b)$, $[\partial\chi_b/\partial r]_{r=r_b}$, and the geometric factors a and b. Generally speaking, the equilibrium flow equation (17) for $\chi_b(r)$ must be integrated with respect to r to determine $\chi_b(r=r_b)$ and $[\partial\chi_b/\partial r]_{r=r_b}$ in Eqs.(20) and (21).

Cylindrical effects are included in Eqs.(20) and (21) in a fully self-consistent manner. As shown in Sec. 7, Eqs.(20) and (21), together with Eq.(17), can be used to determine numerically the normalized layer thickness $\Delta = (r_b - a)/(b-a)$ in terms of the normalized voltage eV/mc^2 and fill field $eB_f(b-a)/mc^2$, and the geometric factors a and b. For completeness, we first consider Eqs.(17), (20) and (21) in the limit of a planar diode.

5. RELATIVISTIC PLANAR FLOW

In the limit of a planar diode with $(b-a)^2 \ll a^2$, $(r_b-a)^2 \ll a^2$ and $\kappa^2a^2 \gg \sinh^2[\chi_b(r=r_b)]$, it is readily shown that the solution to Eq.(17) reduces to the familiar result $\chi_b(r) = \kappa(r-a)$ over the radial extent of the electron layer ($a \leq r < r_b$), and that Eqs.(20) and (21) can be approximated by

$$1 + \frac{eV}{mc^2} = \cosh\left[\kappa(r_b-a)\right] + \kappa(b-r_b)\,\sinh\left[\kappa(r_b-a)\right] , \tag{22}$$

$$\frac{eB_f(b-a)}{mc^2} = \sinh\left[\kappa(r_b-a)\right] + \kappa(b-r_b)\,\cosh\left[\kappa(r_b-a)\right] . \tag{23}$$

For specified value of the normalized fill field $eB_f(b-a)/mc^2$, the voltage eV/mc^2 must be sufficiently small to assure magnetically insulated flow with $r_b < b$, i.e., the outer edge of the electron layer is not in contact with the anode. Examination of Eqs.(22) and

(23) shows that the condition $r_b < b$ requires that the voltage V must be smaller than the Hull cut-off voltage V_H defined by[2,4]

$$\frac{eV_H}{mc^2} = \left[1 + \frac{e^2B_f^2(b - a)^2}{m^2c^4} \right]^{1/2} - 1 . \tag{24}$$

Whenever $V < V_H$, the electron flow is magnetically insulated with $r_b < b$. A plot of eV_H/mc^2 versus normalized fill field $eB_f(b - a)/mc^2$ is presented in Fig. 3 for the case of a planar diode.

For effective interaction between the layer electrons and the RF field in a magnetron, the layer thickness $r_b - a$ should be at least large enough that the (fastest) electrons at $r = r_b$ resonate with the excited waves with phase velocity $v_p = \omega/k_y$. This requires that the voltage V exceed a value[2,4,17] known as the Buneman-Hartree threshold voltage V_{BH}. Equations (22) and (23) can be combined to give

$$\frac{eV}{mc^2} = \frac{eB_f(b - a)}{mc^2} \tanh\left[\kappa(r_b - a)\right] - \left\{1 - \frac{1}{\cosh\kappa(r_b - a)}\right\} . \tag{25}$$

Setting $\beta_b(r = r_b) = \tanh[\kappa(r_b - a)] = \omega/ck_y \equiv \beta_p$, and $\gamma_b(r = r_b) = \cosh\kappa[(r_b - a)] = (1 - \beta_p^2)^{-1/2}$, it is readily shown from Eq.(25) that the Buneman-Hartree threshold voltage V_{BH} is given by

$$\frac{eV_{BH}}{mc^2} = \frac{eB_f(b - a)}{mc^2} \beta_p - \left[1 - (1 - \beta_p^2)^{1/2}\right] . \tag{26}$$

For purposes of illustration, Fig. 3 also shows a plot of eV_{BH}/mc^2 versus normalized fill field $eB_f(b - a)/mc^2$ obtained from Eq.(26) for the choice of phase velocity $\beta_p = v_p/c = 0.8$. The allowed region of magnetron operation ($V_{BH} < V < V_H$) for $\beta_p = 0.8$ then corresponds to the shaded region in Fig. 3.

Equations (22) and (23) can be used to determine closed analytical expressions for $(r_b - a)/b - a)$ and $\kappa(b - a) = \omega_{pb}(a)(b - a)/c$ in terms of eV/mc^2 and $eB_f(b - a)/mc^2$ for the case of a planar diode. Typical results are illustrated in Fig. 4, which shows plots of the normalized layer thickness $(r_b - a)/(b - a)$ versus eV/mc^2 obtained from Eqs.(22) and (23) for values of magnetic fill field ranging from $\tilde{B}_f = eB_f(b - a)/mc^2 = 0.25$ to 8. As the electron flow becomes increasingly relativistic, we note from Fig. 4 that the curves asymptote

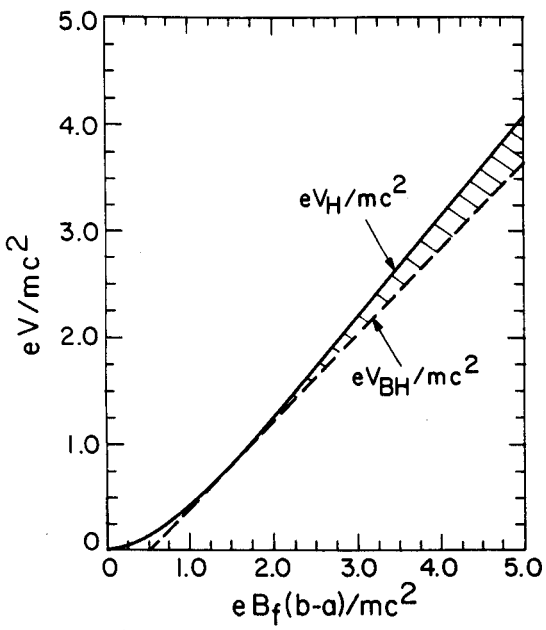

Fig. 3. Plot of the normalized Hull cut-off voltage eV_H/mc^2 versus the normalized fill field $eB_f(b - a)/mc^2$ for a planar diode [Eq.(24)]. The dashed curve corresponds to the normalized Buneman-Hartree voltage eV_{BH}/mc^2 for $\beta_p = 0.8$ [Eq.(26)].

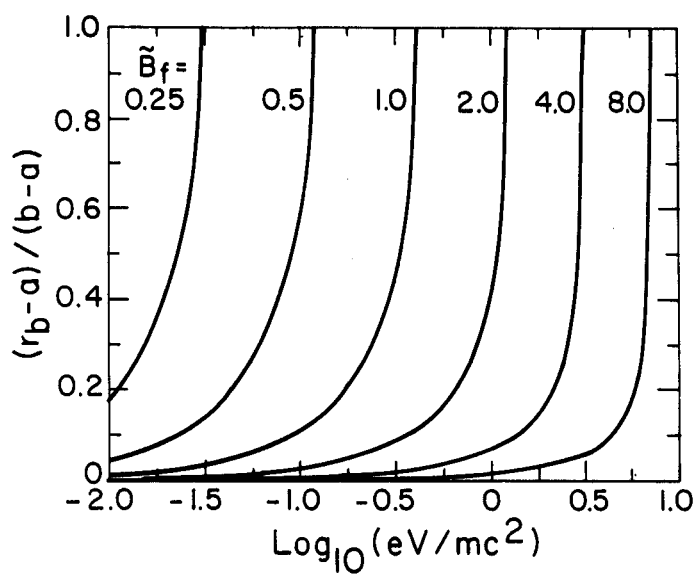

Fig. 4. Plots of the normalized layer thickness $(r_b - a)/(b - a)$ versus $\mathrm{Log}_{10}(eV/mc^2)$ obtained from Eqs.(22) and (23) for a planar diode and several values of the normalized fill field $\tilde{B}_f = eB_f(b - a)/mc^2$.

abruptly as the voltage V approaches the relativistic Hull cut-off voltage defined in Eq.(24). The intercepts for $r_b = b$ and $(r_b - a)/(b - a) = 1$ in Fig. 4 of course correspond to $eV/mc^2 = eV_H/mc^2$.

6. NONRELATIVISTIC CYLINDRICAL FLOW

For nonrelativistic Brillouin flow with $\beta_b^2(r) << 1$ in cylindrical geometry, it is readily shown that $B_z(r) \simeq B_f$ for $a \leq r \leq b$, and the azimuthal flow velocity is given by

$$\beta_b(r) = \frac{1}{2}\frac{\omega_c}{c}\left(\frac{r^2 - a^2}{r}\right) \tag{27}$$

for $a \leq r < r_b$. Moreover, the equilibrium radial electric field $E_r(r)$ and density $n_b(r)$ can be expressed as

$$rE_r(r) = -\frac{B_f\omega_c}{c}\left(\frac{r^4 - a^4}{4r^2}\right) , \tag{28}$$

and

$$\omega_{pb}^2(r) = \omega_c^2\left[1 - \frac{1}{2}\left(\frac{r^4 - a^4}{r^4}\right)\right] , \tag{29}$$

within the electron layer ($a \leq r < r_b$). Here $\omega_c = eB_f/mc$ and $\omega_{pb}^2(r) = 4\pi n_b(r)e^2/m$. For an electron layer with moderate aspect ratio $a/(r_b - a)$, it is clear from Eq.(29) that the radial variation of $\omega_{pb}^2(r)$ can be significant. For example, if $r_b/a = 3/2$, then $\omega_{pb}^2(r)$ decreases monotonically from ω_c^2 at $r = a$ to $(97/162)\omega_c^2$ at $r = r_b$. Poisson's equation (3) can be integrated from $r = a$ to $r = b$ for the equilibrium density profile in Eq.(29). Enforcing $\phi_0(r = b) = V$ gives

$$\frac{eV}{mc^2} = \frac{1}{2}\frac{\omega_c^2}{c^2}\left(\frac{r_b^2 - a^2}{2r_b}\right)^2 + \frac{1}{4}\frac{\omega_c^2}{c^2}\left(\frac{r_b^4 - a^4}{r_b^2}\right)\ln\left(\frac{b}{r_b}\right) , \tag{30}$$

where the nonrelativistic treatment requires $eV/mc^2 << 1$.

For specified values of the normalized voltage eV/mc^2 and magnetic field $eB_f(b - a)/mc^2$, Eq.(30) can be used to determine the normalized layer thickness

$$\Delta_b = \frac{r_b - a}{b - a} . \tag{31}$$

For a diode with moderate aspect ratio, the cylindrical effects incorporated in Eq.(30) can be significant. For example, in the limit where the electron layer extends to the anode ($r_b = b$), the Hull cut-off voltage determined from Eq.(30) is given by

$$\frac{eV_H}{mc^2} = \frac{1}{2}\,\frac{\omega_c^2(b-a)^2}{c^2}\left(\frac{b+a}{2b}\right)^2 . \tag{32}$$

Typical numerical solutions to Eq.(30) are presented in Fig. 5, where $\Delta_b = (r_b - a)/(b - a)$ is plotted versus $(eV/mc^2)/[\omega_c^2(b - a)^2/2c^2]$ for $b/a = 2$, $b/a = 3/2$, and $a/(b - a) = A_d \to \infty$. The curve labelled $A_d = \infty$ in Fig. 5 corresponds to the nonrelativistic limit of a planar diode. As b/a is increased, we note from Fig. 5 that the normalized layer thickness Δ_b increases more rapidly with increasing values of the normalized voltage.

7. RELATIVISTIC CYLINDRICAL FLOW

We now extend the planar analysis in Sec. 5 to include the full influence of cylindrical effects that are incorporated in the relativistic equilibrium flow equation (17) and the expressions for eV/mc^2 and $eB_f(b - a)/mc^2$ in Eqs.(20) and (21). Because Eq.(17) must be solved concurrent with Eqs.(20) and (21) in cylindrical geometry, closed analytical expressions for the normalized layer thickness $(r_b - a)/(b - a)$ are not tractable as in the limit of a planar diode. Therefore, the majority of results obtained for relativistic cylindrical flow are necessarily numerical.

Certain analytical results, however, can be obtained from Eqs.(17), (20) and (21). For example, the Hull cut-off voltage V_H including cylindrical effects[2,4] is readily obtained by setting $r_b = b$ in Eqs.(20) and (21). This gives

$$\frac{eV_H}{mc^2} = \left[1 + g_1^2\,\frac{e^2B_f^2(b-a)^2}{m^2c^4}\right]^{1/2} - 1 , \tag{33}$$

where g_1 is the geometric factor defined by

$$g_1 = \frac{b+a}{2b} . \tag{34}$$

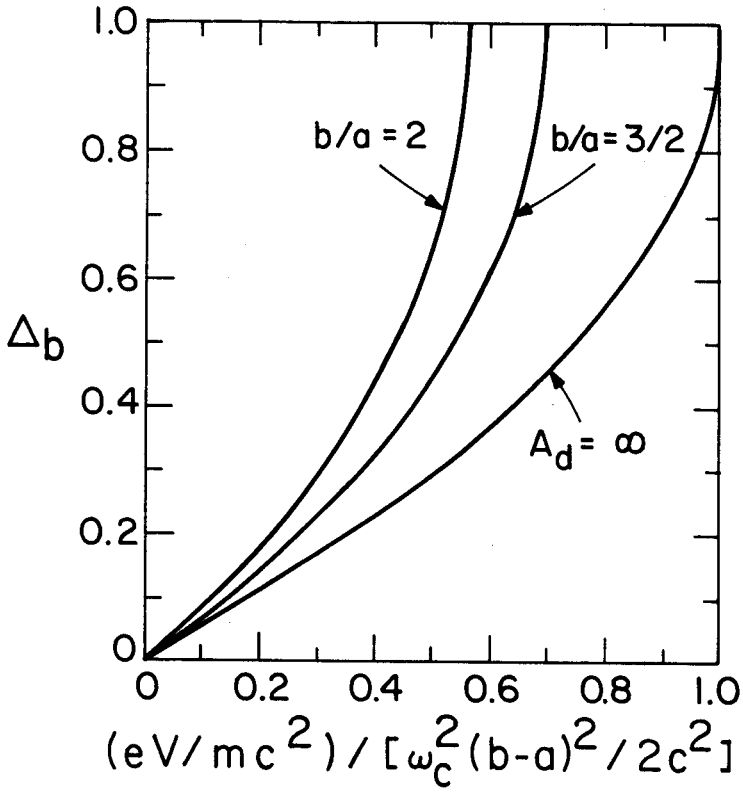

Fig. 5. Plots of the normalized layer thickness $\Delta_b = (r_b - a)/(b - a)$ versus normalized voltage obtained from Eq.(30) for nonrelativistic electron flow in a cylindrical diode and several values of b/a.

For $V < V_H$ defined in Eq.(33), the electron flow in a cylindrical diode is magnetically insulated from contact with the anode. In the limit of a planar diode with $(b - a)^2 << a^2$, the geometric factor $g_1 \rightarrow 1$ in Eq.(34), and Eq.(33) reduces to the planar result in Eq.(24). As b/a is increased, however, g_1 decreases from unity and cylindrical effects become increasingly important. This is illustrated in Fig. 6 where eV_H/mc^2 calculated from Eq.(33) is plotted versus the normalized fill field $eB_f(b - a)/mc^2$ for several values of b/a and the geometric factor $g_1 = (b + a)/2b$. The curve labeled $g_1 = 1$ in Fig. 6 corresponds to the planar limit of a diode with infinite aspect ratio, i.e., $A_d = a/(b - a) \rightarrow \infty$ [see Eq.(24) and Fig. 3]. As b/a is increased and therefore g_1 is reduced, it is clear from Eq.(33) and Fig. 6 that cylindrical effects reduce the Hull cut-off voltage relative to the planar estimate in Eq.(24) and Fig. 3. From Eq.(34),

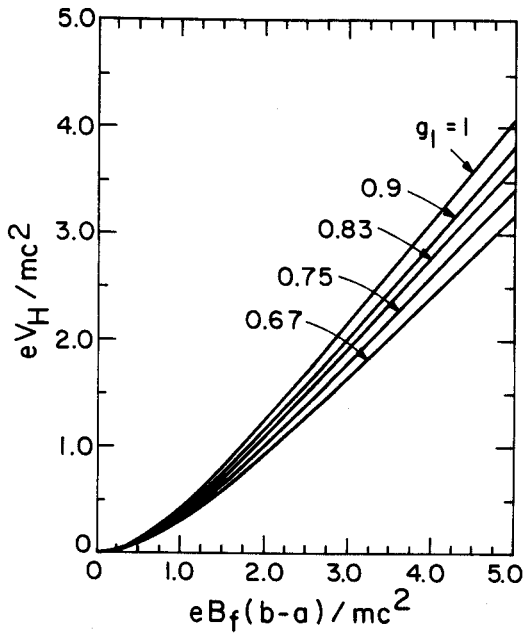

Fig. 6. Plots of the normalized Hull cut-off voltage eV_H/mc^2 versus the normalized fill field $eB_f(b - a)/mc^2$ for relativistic electron flow in a cylindrical diode and several values of the geometric factor $g_1 = (b + a)/2b$ [Eq.(33)].

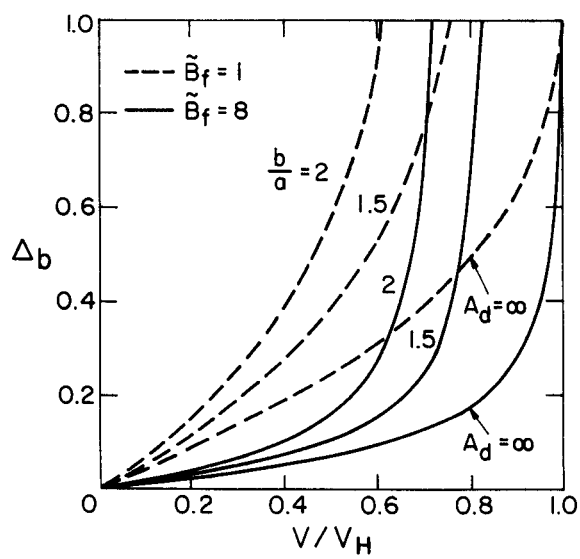

Fig. 7. Plots of the normalized layer thickness $\Delta_b = (r_b - a)/(b - a)$ versus the normalized voltage V/V_H obtained from Eqs.(17), (20) and (21) for relativistic electron flow in a cylindrical diode. Here, V_H is <u>planar</u> Hull cut-off voltage defined in Eq.(24).

this reduction factor is equal to $1 - g_1^2$ in the nonrelativistic regime and equal to $1 - g_1$ in the highly relativistic regime where $eV_H/mc^2 >> 1$. The associated reduction in eV_H/mc^2 can be substantial for moderate values of b/a. For example, if b/a = 3, then $g_1 = 2/3$, and $1 - g_1^2 = 5/9$ and $1 - g_1 = 1/3$.

Equations (17), (20) and (21) have been solved numerically to determine the scaling of the normalized layer thickness $\Delta_b = (r_b - a)/(b - a)$ with voltage eV/mc^2 and fill field $\tilde{B}_f = eB_f(b - a)/mc^2$. Typical numerical results are illustrated in Fig. 7, where Δ_b is plotted versus V/V_H for $\tilde{B}_f = 1$ (dashed curves) and $\tilde{B}_f = 8$ (solid curves) and b/a = 2, 3/2 and $A_d = a/(b - a) \rightarrow \infty$. In Fig. 7, the voltage V is normalized to the relativistic <u>planar</u> Hull cut-off voltage V_H defined in Eq.(24). As in the case of nonrelativistic, cylindrical flow (Fig. 5), the normalized layer thickness Δ_b exhibits a strong dependence on cylindrical effects as measured by b/a. Moreover, for each case presented in Fig. 7, Δ_b approaches unity whenever V approaches the relativistic <u>cylindrical</u> Hull cut-off voltage V_H defined in Eq.(33). Evidently, when relativistic effects are strong (the $\tilde{B}_f = 8$ case in Fig. 7), Δ_b approaches unity more abruptly than when the flow is nonrelativistic (compare with Fig. 5).

8. CONCLUSIONS

A macroscopic cold-fluid model has been used to determine the influence of cylindrical effects on the operating range and properties of the electron flow in relativistic smooth-bore magnetrons. Assuming operation at Brillouin flow [Eq.(9)], it is found that cylindrical effects can significantly modify several features of the equilibrium flow and diode operating range relative to the case of planar flow. For example, centrifugal effects reduce the radial electric field (and therefore the Hull cut-off voltage V_H) required to fill the cathode-anode gap with $r_b = b$ [see Fig. 6]. The normalized layer thickness $\Delta_b = (r_b - a)/(b - a)$ has been calculated over a wide range of system parameters b/a, eV/mc^2 and $eB_f(b - a)/mc^2$ [Fig. 7].

9. ACKNOWLEDGMENTS

This research was supported by the Innovative Science and Technology Office of SDIO and managed by Harry Diamond Laboratories.

10. REFERENCES

1. J. Benford, in High-Power Microwave Sources, edited by V. Granatstein and I. Alexeff (Artech House, 1987), Chapter 10.
2. Y.Y. Lau, in High-Power Microwave Sources, edited by V. Granatstein and I. Alexeff (Artech House, 1987), Chapter 9.
3. A. Palevsky, G. Bekefi and A.T. Drobot, J. Appl. Phys. 52, 4938 (1981).
4. A. Palevsky and G. Bekefi, Phys. Fluids 22, 986 (1979).
5. T.J. Orzechowski and G. Bekefi, Phys. Fluids 22, 978 (1979).
6. G. Bekefi and T.J. Orzechowski, Phys. Rev. Lett. 37, 379 (1976).
7. T.M. Antonsen, Jr. and E. Ott, Phys. Fluids 19, 52 (1976).
8. E. Ott and R.V. Lovelace, Appl. Phys. Lett. 27, 378 (1975).
9. C.L. Chang, E. Ott and T.M. Antonsen, Jr., Phys. Fluids 29, 3851 (1986).
10. R.C. Davidson and K.T. Tsang, Phys. Fluids 28, 1169 (1985).
11. R.C. Davidson, K.T. Tsang and J.A. Swegle, Phys. Fluids 27, 2332 (1984).
12. C.L. Chang, T.M. Antonsen, Jr., E. Ott and A.T. Drobot, Phys. Fluids 27, 2545 (1984).
13. J. Swegle and E. Ott, Phys. Fluids 24, 1821 (1981).
14. K.T. Tsang and R.C. Davidson, Phys. Rev. A33, 4284 (1986).
15. R.C. Davidson and K.T. Tsang, Phys. Fluids 29, 3832 (1986).
16. D. Chernin and Y.Y. Lau, Phys. Fluids 27, 2319 (1984).
17. O. Buneman, in Cross-Field Microwave Devices, edited by E. Okress (Academic, New York, 1961), Vol. 1, p. 209.